Available online at www.sciencedirect.com

ScienceDirect

Procedia Structural Integrity 1 (2016) 042–049

Structural Integrity Procedia

www.elsevier.com/locate/procedia

XV Portuguese Conference on Fracture, PCF 2016, 10-12 February 2016, Paço de Arcos, Portugal

Numerical evaluation of dissimilar cohesive models to predict the behavior of Double-Cantilever Beam specimens

R.L. Fernandes[a], R.D.S.G. Campilho[a,b]*

[a]*Departamento de Engenharia Mecânica, Instituto Superior de Engenharia do Porto, Instituto Politécnico do Porto, Rua Dr. António Bernardino de Almeida, 431, 4200-072 Porto, Portugal*

[b]*INEGI – Pólo FEUP, Rua Dr. Roberto Frias, s/n, 4200-465 Porto, Portugal*

Abstract

Adhesive bonding is a widely used joining method in industries such as aerospace, aeronautical and automotive because of specific advantages compared to the traditional fastening methods. Numerical approaches for the damage simulation of bonded joints based on fracture mechanics usually rely on Cohesive Zone Models (CZM). CZM suppose the characterization of the CZM laws in tension and shear, which are combined in mixed-mode criteria to predict the strength of bonded joints. This work evaluated the tensile fracture toughness (G_{IC}) and CZM laws of bonded joints for two adhesives with distinct ductility. The Double-Cantilever Beam (DCB) test was used. The experimental work consisted of the tensile fracture characterization by the *J*-integral technique. A digital image correlation method was used for the evaluation of the tensile relative displacement (δ_n) of the adhesive layer at the crack tip. Finite Element (FE) simulations were carried out to assess the accuracy of triangular, trapezoidal and linear-exponential CZM laws in predicting the experimental behaviour of the DCB tests. As output of this work, information regarding the applicability of these CZM laws to each type of adhesive is provided, allowing the subsequent strength prediction of bonded joints.

Peer-review under responsibility of the Scientific Committee of PCF 2016.

Keywords: Cohesive zone modelling; J-integral; Finite element analysis; Crack growth, Adhesive joints.

1. Introduction

Adhesive bonding is a widely used joining method in industries such as aerospace, aeronautical and automotive to attach structural components and as repair technique, because of specific advantages compared to the traditional

* Corresponding author. Tel.: +351939526892; fax: +351228321159.
E-mail address: raulcampilho@gmail.com

Peer review under responsibility of the Scientific Committee of PCF 2016.
10.1016/j.prostr.2016.02.007

fastening methods. Many joining and repair configurations are available to the designer, among which single-lap, double-lap or scarf joints are the most typical (Li et al. 2015). Joining with adhesives offers potential to decrease weight and reduces the number of stress raisers, such as the holes that are necessary for fastening and riveting techniques. The generalized use of adhesive bonding in high responsibility structures brings the need to accurately predict the fracture behaviour of bonded structures. Fracture mechanics-based predictive techniques for adhesive joints are better suited that continuum mechanics methods, since the failure of adhesive layers is mostly governed by values of G_{IC} or shear fracture toughness (G_{IIC}) (Ripling et al. 1964). Numerical approaches for the damage simulation of bonded joints based on fracture mechanics can rely either on the Virtual Crack Closure Technique (VCCT) or, more usually, on CZM (Floros et al. 2015). CZM suppose the characterization of the CZM laws in tension and shear, which are afterwards combined in mixed-mode criteria for damage initiation and growth to predict the strength of bonded joints. Softening onset is commonly predicted by stress criteria, while crack propagation, i.e., failure of the CZM element, is usually ruled by energetic criteria. This feature permits simulating structures with complex geometry and loadings with virtually no limitations (Fernandes et al. 2015). Based on previous evidence, the quadratic stress criterion for damage initiation and linear energetic criterion for crack growth work quite well with most structural adhesives. This technique can be used to simulate delaminations in composite structures (Alfano and Crisfield 2001), cohesive failures of wood elements and bondline failures in adhesively-bonded elements (Campilho et al. 2011). Moreover, it is specifically adapted to bonded joints because of the typically mixed-Mode failure occurring in these joints, which is accurately modelled by proper criteria to couple tension and shear (Fernandes et al. 2015). CZM were introduced by Dugdale (1960) and Barenblatt (1959), which associated fracture to the development of a fracture process zone (FPZ) that develops at the vicinity of the crack tip in metals. The allowable dimension of this FPZ, above which crack propagates catastrophically, is dependent on the fracture toughness (G_C) of the cracked material. This concept can be extended to crack growth in adhesively-bonded joints, with the difference that the FPZ's extent is intrinsically limited by the neighbouring adherends, thus only spanning through the adhesive layer. This makes G_C dependent on the degree of restriction to the deformations in the adhesive layer, i.e., these quantities are adhesive thickness (t_A) and adherend thickness (t_P) dependent. CZM relate the tensile (t_n) and shear cohesive stress (t_s) of the adhesive as a function of δ_n and shear relative displacement (δ_s) between homologous nodes of the cohesive elements.

Mainly three methods can be used to derive the CZM laws: the property identification technique, the inverse method and the direct method, each of these with specific advantages and limitations. The property identification method consists of individually characterizing each one of the CZM parameters by specific tests. The inverse method is based on tuning the CZM parameters by comparing the simulation results, e.g., the load-displacement (P-δ) curve of pure-Mode fracture tests, to the respective experimental results (Campilho et al. 2009). Finally, the direct method consists of the measurement of the tensile (G_I) or shear strain energy release rate (G_{II}) by the J-integral and values of δ_n and δ_s by a physical or optical technique (Campilho et al. 2013a), and subsequent differentiation of the G_I–δ_n or G_{II}–δ_s curves (Leffler et al. 2007). In the direct method, it is only necessary to plot these curves up to crack onset, because the predicted value of G_{IC} or G_{IIC} corresponds to the steady-state value of G_I or G_{II} that is attained when the crack begins to propagate.

Few works focus on the optimal CZM law shape to model adhesive layers and, although using a CZM law that is not particularly tailored for a given adhesive may still give a rough prediction of the bonded structures' behaviour (Campilho et al. 2013b), for best results in the strength prediction, care must be taken for the proper selection of the CZM shape. Fernandes et al. (2015) addressed the tensile behaviour of single-lap joints between aluminium adherends and different overlap lengths, with three adhesives of distinct ductility: the brittle epoxy Araldite® AV138, the moderately ductile epoxy Araldite® 2015 and the ductile polyurethane Sikaforce® 7888. An extensive CZM analysis was undertaken by using a triangular CZM for all adhesives, whose properties were found either by the property identification or inverse techniques. Whilst the results were accurate for all joint configurations bonded with the Araldite® AV138 and 2015 (alternating between deviations by defect or excess, and with maximum percentile deviations of 9.8% for the Araldite® AV138 and 7.7% for the Araldite® 2015), consistent under predictions for all overlap lengths were detected for the Sikaforce® 7888 at nearly 20%. It was concluded that this was due to excessive softening in the CZM laws representing the adhesive's behaviour when yielding was attained.

This work evaluated the value of G_{IC} and CZM laws of bonded joints for two adhesives with distinct ductility. The DCB test geometry was used with this purpose. The experimental work consisted on the tensile fracture characterization of the bond by the J-integral technique. Additionally, the precise shape of the cohesive law was

defined. FE simulations were carried out in Abaqus® to assess the accuracy of the triangular, trapezoidal and linear-exponential CZM laws in predicting the experimental behaviour of the DCB tests.

2. Experimental part

2.1. Materials

The aluminium alloy AA6082 T651 was chosen for the adherends, whose tensile mechanical properties were obtained in the work of Campilho et al. (2011): Young's modulus (E) of 70.07±0.83 GPa, tensile yield stress (σ_y) of 261.67±7.65 MPa, tensile failure strength (σ_f) of 324±0.16 MPa and tensile failure strain (ε_f) of 21.70±4.24%. Two structural adhesives were considered: the brittle epoxy Araldite® AV138 and the ductile polyurethane Sikaforce® 7752. These adhesives were previously characterized (Campilho et al. 2013b, Campilho et al. 2011, Faneco et al. 2015). Bulk specimens were tested to obtain E, σ_y, σ_f and ε_f. The DCB test was selected to obtain G_{IC} and the End-Notched Flexure (ENF) test for G_{IIC}. The collected data of the adhesives is summarized in Table 1.

Table 1 – Properties of the adhesives Araldite® AV138 and Sikaforce® 7752 (Campilho et al. 2013b, Campilho et al. 2011, Faneco et al. 2015).

Property	**AV138**	**7752**
Young's modulus, E [GPa]	4.89±0.81	0.49±0.09
Poisson's ratio, ν	0.35 [a]	0.30 [a]
Tensile yield stress, σ_y [MPa]	36.49±2.47	3.24±0.48
Tensile failure strength, σ_f [MPa]	39.45±3.18	11.48±0.25
Tensile failure strain, ε_f [%]	1.21±0.10	19.18±1.40
Shear modulus, G [GPa]	1.56±0.01	0.19±0.01
Shear yield stress, τ_y [MPa]	25.1±0.33	5.16±1.14
Shear failure strength, τ_f [MPa]	30.2±0.40	10.17±0.64
Shear failure strain, γ_f [%]	7.8±0.7	54.82±6.38
Toughness in tension, G_{IC} [N/mm]	0.20 [b]	2.36±0.17
Toughness in shear, G_{IIC} [N/mm]	0.38 [b]	5.41±0.47

[a] manufacturer's data

[b] estimated in Campilho et al. (2011)

2.2. Specimen geometry

The DCB test was selected to estimate G_{IC} (Fig. 1). The aluminum alloy sheet AA6082 T651 was considered for the adherends, cut to the dimensions of 140×25×3 mm^3. The chosen dimensions for the DCB joint are: total length L=140 mm, initial crack length a_0≈55 mm, t_P=3 mm, t_A=1 mm and width B=25 mm.

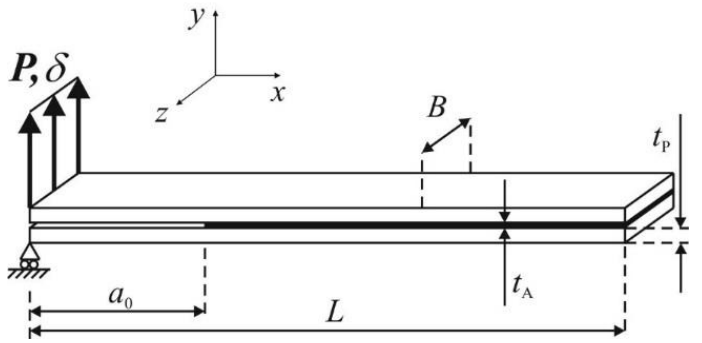

Fig. 1 – Geometry of the DCB specimens.

The preparation of the DCB specimens involved painting the crack path and attaching a printed scale to enable measuring the crack length (a) during the tests or input data for the digital correlation technique. Six DCB specimens

were tested in a Shimadzu AG-X 100 testing machine with a load cell of 100 kN. Each test was fully documented using an 18 MPixel digital camera with no zoom and fixed focal distance to approximately 100 mm. This procedure allowed obtaining the values of δ_n and adherends rotation at the crack tip (θ_o).

2.3. Direct method for CZM law estimation

Based on the fundamental expression for J (Rice 1968), it is possible to derive an expression for G_I applied to the DCB specimen from the concept of energetic force and also the beam theory, as follows (Zhu et al. 2009)

$$G_I = 12\frac{\left(P_u a\right)^2}{E t_P^{\,3}} + P_u \theta_o \quad \text{or} \quad G_I = P_u \theta_p, \tag{1}$$

where P_u represents the applied load per unit width at the adherends' edges and θ_p the adherends' rotation at the loading point. G_{IC} can be considered the value of G_I at the beginning of crack growth. Thus, G_{IC} is given by the steady-state value of G_I, at a δ_n value equal to the tensile failure displacement (δ_n^f) (Ji et al. 2010). The $t_n(\delta_n)$ curve can be obtained by differentiation of equation (1) with respect to δ_n

$$t_n\left(\delta_n\right) = \frac{\mathrm{d}G_I}{\mathrm{d}\delta_n}. \tag{2}$$

For the implementation of this technique, a previously developed algorithm was used (Campilho et al. 2014), based on digital image processing and tracking reference points by the software to give estimated measurements of θ_o and δ_n. The details of the point tracking algorithm used to automatically track the points of each picture of a given test, after the points in the first figure of the test are manually identified, and the formulae to define θ_o and δ_n, are presented in the reference of Campilho et al. (2014).

3. Numerical part

A numerical analysis of the DCB joints was performed in the FE software ABAQUS® to assess the suitability of the triangular, linear-exponential and trapezoidal CZM laws in predicting the tensile behavior of the DCB bonded joints. The numerical analysis was carried out using non-linear geometrical considerations using the material properties defined in Section 2.1. The adherends were modelled with plane-strain 8-node quadrilateral solid finite elements and the adhesive layer with a single row of 4-node cohesive elements. Six solid finite elements were used through-thickness in each arm, with a more refined mesh near the adhesive region. The meshes were constructed taking advantage of the automatic meshing capabilities of ABAQUS®, namely bias effects, which allow grading the elements' size in the adherends from the loading points towards the crack tip, and also vertically in the direction of the adhesive layer, where large stress gradients are expected. As boundary conditions, the lower edge node of the lower arm was fixed, and a vertical displacement and horizontal restriction was applied to the upper edge node of the upper arm. For each test, the three types of CZM laws under study were built with the value of tensile cohesive strength (t_n^0) and G_{IC} obtained for the respective specimen by the direct method. For a full description of the formulation of the CZM laws, the reader can refer to the work of Campilho et al. (2013b).

4. Results

4.1. Estimation of G_{IC} and CZM laws

The values of G_{IC} by the J-integral were estimated from equation (1), using the left expression with θ_o instead of θ_p. Fig. 2 pictures a G_{IC}-δ_n curve for a DCB test of each adhesive. The curve of the Araldite® AV138 is represented in the vertical axis at the right because of the smaller G_{IC} values, and the x-axis is truncated at δ_n=0.12 mm to improve

visualization. The polynomial curves to derive the CZM laws by differentiation of the G_{IC}-δ_n curves are overlapped to the experimental data.

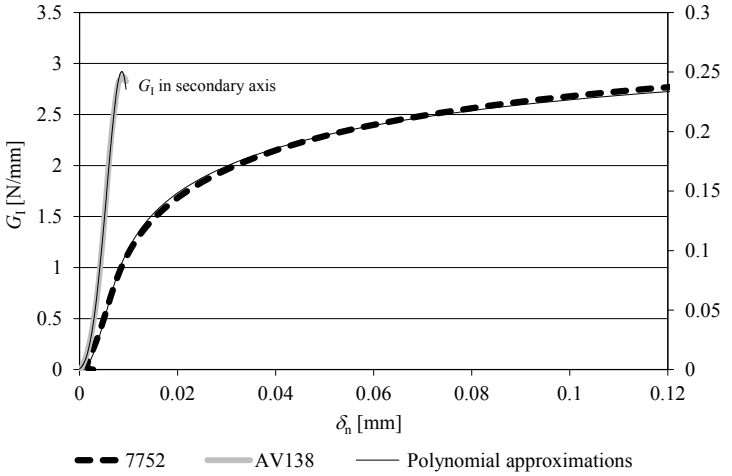

Fig. 2 – Representative G_{IC}-δ_n laws for each tested adhesive and respective polynomial approximations.

Table 2 – Values of G_{IC} [N/mm] for the two adhesives obtained by all methods (Constante et al. 2015, Campilho et al. 2015).

Adhesive	Araldite® AV138				Sikaforce® 7752	
Specimen	CCM	CBT	CBBM	*J*-integral	CBBM	*J*-integral
1	0.200	0.237	0.231	0.224	3.420	3.420
2	0.219	0.241	0.247	0.252	3.903	3.900
3	0.193	0.215	0.234	0.231	3.842	3.840
4	--	0.291	0.310	0.329	4.183	4.000
5	0.189	0.237	0.254	0.237	3.247	3.400
6	0.195	0.206	0.217	0.197	3.502	3.650
Average	0.199	0.238	0.249	0.245	3.683	3.702
Deviation	0.012	0.030	0.033	0.045	0.320	0.231

G_{IC} is calculated by the steady-state value of G_I in the G_I-δ_n curve (Fig. 2). Comparing the curves between adhesives, it is clearly visible that the value of δ_n correspondent to the stabilization point increases with the adhesive ductility, which will correspond to higher δ_n^f values in the respective CZM laws. On the other hand, the Sikaforce® 7752 curve reveals softening near to G_{IC} because of its ductility, oppositely to what happens with the Araldite® AV138.

Table 2 summarizes the obtained results and compares them with conventional techniques such as the Compliance Calibration Method (CCM), Corrected Beam Theory (CBT) and Compliance-Based Beam Method (CBBM) applied to the same specimens in previous works (Constante et al. 2015, Campilho et al. 2015). For the Sikaforce® 7752, only the CBBM is available as conventional method. The G_{IC} values compare well between methods. The application of equation (2) to the G_I-δ_n curves gives the CZM law estimation. Fig. 3 shows a representative t_n-δ_n or CZM law for each adhesive (corresponding to the G_I-δ_n curves of Fig. 2), equally truncating the *x*-axis at δ_n=0.12 to improve visualization. The obtained CZM law of the Araldite® AV138 is adjusted best by a triangular simplified law on account of its brittleness, while the law of the Sikaforce® 7752 is overlapped with a simplified trapezoidal law, which provides the best match because of these adhesives' ductility.

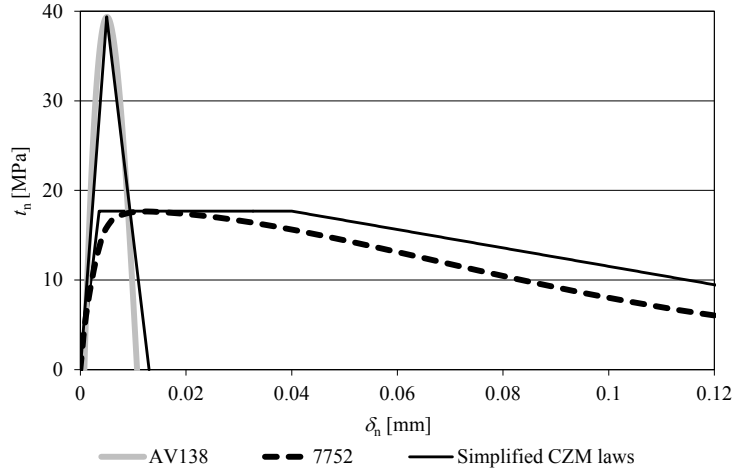

Fig. 3 – Representative t_n-δ_n or CZM laws for each tested adhesive and simplified CZM laws.

4.2. Effect of the CZM law shape

Fig. 4 shows the fitting procedure of selected experimental CZM laws for each adhesive with triangular, trapezoidal and linear-exponential laws. The comparison shows that the Araldite® AV138 is best modelled by a triangular CZM law rather than trapezoidal or linear-exponential. Oppositely, the Sikaforce® 7752 tensile behaviour is more accurately reproduced by a trapezoidal CZM law. The linear-exponential law is not suited for any of the adhesive.

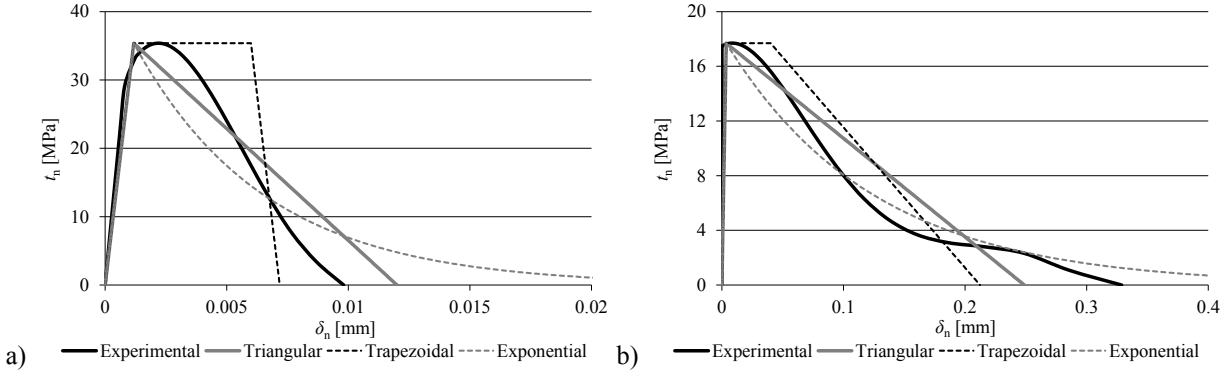

Fig. 4 – Reproduction of the CZM laws with triangular, trapezoidal and linear-exponential laws: Araldite® AV138 (a) and Sikaforce® 7752 (b).

Fig. 5 displays the simulation results for the three CZM shapes under evaluation for the same specimens of Fig. 4, with the respective experimental curve. For the Araldite® AV138, the three law shapes have an identical evolution of P during crack growth. The similar behaviour during propagation is justified by this stage in DCB specimens being ruled by G_{IC}. The only difference regards near the maximum load (P_{max}). At this zone, the linear-exponential law has a smaller value. For the Araldite® AV138, the triangular law has an average error of absolute values of 7.69% in P_{max} and 2.62% in the maximum load displacement (δP_{max}). The trapezoidal law has corresponding errors of 4.38% and 4.45%. The linear-exponential law has the worst results with errors of 13.55% and 8.25%, by the same order, which is linked to excessive softening registered in this specific CZM law shape after attaining t_n^0.

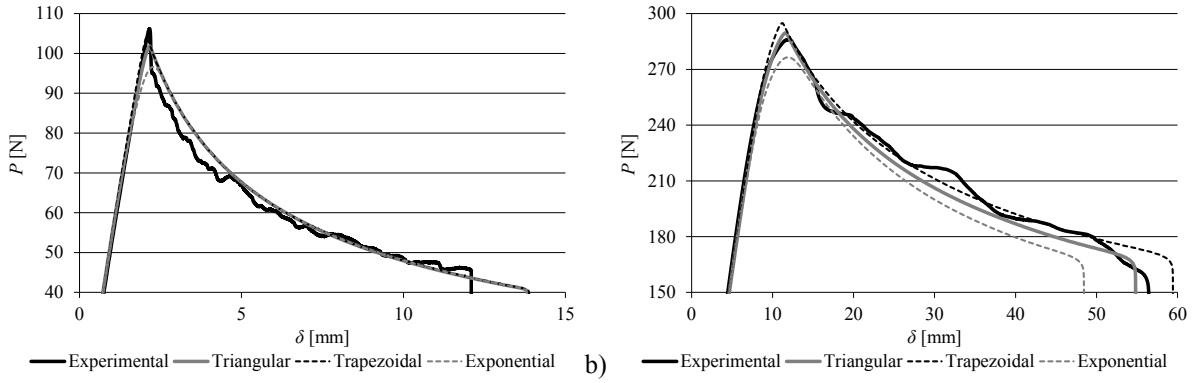

Fig. 5 – Comparison between the experimental P-δ curves with the numerical predictions: Araldite® AV138 (a) and Sikaforce® 7752 (b).

It was found that, for the Sikaforce® 7752, the triangular and exponential CZM laws consistently under predicted the P values during crack growth comparatively to the experimental P-δ curves. On the other hand, the trapezoidal law was accurate in capturing the experimental results. It is considered that this difference arises from the high ductility of this particular adhesive. In average, the percentile deviations between the experimental and numerical values of P_{max} and δP_{max} are the following: 2.16% and 3.44% (triangular CZM law), 3.14% e 6.07% (trapezoidal CZM law) and 12.21% and 3.37% (linear-exponential CZM law). In summary, for adhesives other than highly ductile, the crack growth behavior is not affected by the CZM law shape and, thus, any law is applicable, which reinforces the previously mentioned statement that in pure tension the strength predictions are practically independent of the CZM law shape. On the other hand, crack initiation in bonded structures is affected by the CZM law, with the linear-exponential law triggering premature failure, especially for ductile adhesives.

5. Conclusions

This work initially aimed at evaluating G_{IC} and the tensile CZM law of two structural adhesives with distinct ductility. This was accomplished by performing fracture tests on DCB specimens and using the J-integral/direct method. G_{IC} was assessed by the steady-state values of G_I in the respective G_I-δ_n curve of each specimen, giving consistent values with the adhesive type and known behaviour from the literature. The obtained CZM laws showed a best fit of the Araldite® AV138 with a triangular law, while the Sikaforce® could be more accurately represented by a trapezoidal CZM law due to its ductility. The numerical simulations enabled a clear insight regarding the best CZM law shape to model the tensile behaviour of each adhesive in bonded joints. The propagation region in the P-δ curves for the Araldite® AV138 was not affected by the CZM shape, oppositely to what happened with Sikaforce® 7752, in which the triangular and linear exponential CZM laws revealed to under predict P during crack growth. This discrepancy was associated to the large ductility of the adhesive. P_{max} and δP_{max} were also used as indications of approximation to the experiments. The absolute errors in these values were close between the triangular and trapezoidal laws for the Araldite® AV138, while the linear-exponential CZM law resulted in excessive softening in the initial stages of damage and thus, bigger deviations in the results. The P_{max} values were also highly under predicted with a linear-exponential CZM law. The general conclusion taken from this work is that, if the adhesive is not highly ductile, the adhesives' behaviour during crack growth can be correctly modelled by any CZM law shape. On the other hand, crack initiation is anticipated by using linear-exponential CZM laws.

References

Li, J., Yan, Y., Zhang, T. and Liang, Z. 2015. Experimental study of adhesively bonded CFRP joints subjected to tensile loads. International Journal of Adhesion and Adhesives 57: 95-104.

Ripling, E., Mostovoy, S. and Patrick, R. 1964. Application of fracture mechanics to adhesive joints. ASTM Special Technical Publication 360: 5-19.

Floros, I. S., Tserpes, K. I. and Löbel, T. 2015. Mode-I, mode-II and mixed-mode I+II fracture behavior of composite bonded joints: Experimental characterization and numerical simulation. Composites Part B: Engineering 78: 459-468.

Fernandes, T. A. B., Campilho, R. D. S. G., Banea, M. D. and da Silva, L. F. M. 2015. Adhesive selection for single lap bonded joints: Experimentation and advanced techniques for strength prediction. The Journal of Adhesion 91: 841-862.
Alfano, G. and Crisfield, M. A. 2001. Finite element interface models for the delamination analysis of laminated composites: mechanical and computational issues. International Journal for Numerical Methods in Engineering 50: 1701-1736.
Campilho, R. D. S. G., Banea, M. D., Pinto, A. M. G., da Silva, L. F. M. and de Jesus, A. M. P. 2011. Strength prediction of single- and double-lap joints by standard and extended finite element modelling. International Journal of Adhesion and Adhesives 31: 363-372.
Dugdale, D. S. 1960. Yielding of steel sheets containing slits. Journal of the Mechanics and Physics of Solids 8: 100-104.
Barenblatt, G. I. 1959. The formation of equilibrium cracks during brittle fracture. General ideas and hypothesis. Axisymmetrical cracks. Journal of Applied Mathematics and Mechanics 23: 622-636.
Campilho, R. D. S. G., de Moura, M. F. S. F., Pinto, A. M. G., Morais, J. J. L. and Domingues, J. J. M. S. 2009. Modelling the tensile fracture behaviour of CFRP scarf repairs. Composites Part B: Engineering 40: 149-157.
Campilho, R. D. S. G., Moura, D. C., Gonçalves, D. J. S., da Silva, J. F. M. G., Banea, M. D. and da Silva, L. F. M. 2013a. Fracture toughness determination of adhesive and co-cured joints in natural fibre composites. Composites Part B: Engineering 50: 120-126.
Leffler, K., Alfredsson, K. S. and Stigh, U. 2007. Shear behaviour of adhesive layers. International Journal of Solids and Structures 44: 530-545.
Campilho, R. D. S. G., Banea, M. D., Neto, J. A. B. P. and da Silva, L. F. M. 2013b. Modelling adhesive joints with cohesive zone models: effect of the cohesive law shape of the adhesive layer. International Journal of Adhesion and Adhesives 44: 48-56.
Faneco, T. M. S., Campilho, R. D. S. G., da Silva, F. J. G. and Lopes, R. M. 2015. Strength and fracture characterization of a novel polyurethane adhesive for the automotive industry. Journal of Testing and Evaluation Submitted.
Rice, J. R. 1968. A path independent integral and the approximate analysis of strain concentration by notches and cracks. Journal of Applied Mechanics 35: 379-386.
Zhu, Y., Liechti, K. M. and Ravi-Chandar, K. 2009. Direct extraction of rate-dependent traction–separation laws for polyurea/steel interfaces. International Journal of Solids and Structures 46: 31-51.
Ji, G., Ouyang, Z., Li, G., Ibekwe, S. and Pang, S.-S. 2010. Effects of adhesive thickness on global and local Mode-I interfacial fracture of bonded joints. International Journal of Solids and Structures 47: 2445-2458.
Campilho, R. D. S. G., Moura, D. C., Banea, M. D. and da Silva, L. F. M. 2014. Adherend thickness effect on the tensile fracture toughness of a structural adhesive using an optical data acquisition method. International Journal of Adhesion and Adhesives 53: 15-22.
Constante, C. J., Campilho, R. D. S. G. and Moura, D. C. 2015. Tensile fracture characterization of adhesive joints by standard and optical techniques. Engineering Fracture Mechanics 136: 292-304.
Campilho, R. D. S. G., Moura, D. C., Banea, M. D. and da Silva, L. F. M. 2015. Adhesive thickness effects of a ductile adhesive by optical measurement techniques. International Journal of Adhesion and Adhesives 57: 125-132.